

Corrosion Inhibition Studies of Benzoxazole Derivates for N80 Steel in 1 M HCl Solution: Synthesis, Experimental, and DTF Studies

Dongqiu Yang¹, Xiaojun Feng¹, Ning Yan¹, Yanqun Wang¹, Lilin Lu², Ping Mei¹, Wu Chen¹, Lu Lai^{1*}

¹College of Chemistry and Environmental Engineering, Yangtze University, Jingzhou, China

²College of Chemistry and Chemical Engineering, Wuhan University of Science and Technology, Wuhan, China

Email: *lailuchem@163.com

How to cite this paper: Yang, D.Q., Feng, X.J., Yan, N., Wang, Y.Q., Lu, L.L., Mei, P., Chen, W. and Lai, L. (2022) Corrosion Inhibition Studies of Benzoxazole Derivates for N80 Steel in 1 M HCl Solution: Synthesis, Experimental, and DTF Studies. *Open Journal of Yangtze Gas and Oil*, 7, 101-123. <https://doi.org/10.4236/ojogas.2022.72007>

Received: January 7, 2022

Accepted: February 26, 2022

Published: March 1, 2022

Copyright © 2022 by author(s) and Scientific Research Publishing Inc. This work is licensed under the Creative Commons Attribution International License (CC BY 4.0).

<http://creativecommons.org/licenses/by/4.0/>



Open Access

Abstract

Three benzoxazole corrosion inhibitors, namely 2-(benzo [d]oxazol-2-yl)phenol (BOP), 6-(benzo [d]oxazol-2-yl)pyridin-2-ol (BOPO), and 2-(quinolin-2-yl)benzo [d]oxazole (QBO), were synthesized. Moreover, their corrosion inhibition performance for N80 steel in 1 M HCl solution at 303 K was measured by the electrochemical measurements and surface analysis studies. The results show that the inhibition efficiency of all corrosion inhibitors increases with the increase of concentration. At the same concentration, the order of inhibition efficiency is BOP < BOPO < QBO. Moreover, the studied inhibitors act as mixed-type inhibitors, and the adsorption of all inhibitors on N80 steel followed the Langmuir adsorption isotherm. Further, we have examined the effect of iodide ions on inhibition efficiency. The results show that BOP and KI are synergistic, BOPO and QBO are competitive adsorptions with KI. The quantum chemical parameters such as highest occupied molecular orbital, lowest unoccupied molecular orbital energy levels, and energy gap were calculated by the density functional theory (DFT). The relations between the inhibition efficiency and some quantum parameters have been discussed. The protective effect of the three inhibitors followed the sequence of BOP < BOPO < QBO. The results obtained from quantum chemicals and electrochemical were in reasonable agreement.

Keywords

N80 Steel, Benzoxazole Derivates, Corrosion Inhibition, Electrochemical Measurements, DFT

1. Introduction

It is of practical significance and great value to study the corrosion and protection technology of oil and gas fields [1]. Therefore, some measures, such as surface coatings, electrochemical protection, corrosion inhibitors, have been applied in metal protection. Among these technologies, corrosion inhibitors are widely used in metal protection due to their advantages of economy, efficiency, and convenience [2] [3]. So far, a large number of corrosion inhibitors have been explored and applied in different industrial fields. Among these corrosion inhibitors, heterocyclic compounds efficiently provide electrons to the iron surface, forming coordination bonds and thus enhancing adsorption because of their heterocyclic atoms and conjugated system. Hence, heterocyclic compounds usually have excellent corrosion inhibition performance [4] [5].

Benzoxazole and its derivatives are common heterocyclic compounds and have been used as corrosion inhibitors. Given the facts mentioned above, in this article, three benzoxazole derivatives namely 2-(benzo [d]oxazol-2-yl)phenol (BOP), 6-(benzo [d]oxazol-2-yl)pyridine-2-ol (BOPO), and 2-(quinoline-2-yl)benzo [d]oxazole (QBO) were synthesized. The corrosion inhibition properties of the three inhibitors for N80 steel in 1 M HCl solution were surveyed by polarization curves and electrochemical impedance spectroscopy (EIS). Fourier transform infrared (FT-IR), Field emission scanning electron microscope (FE-SEM), as well as X-ray diffraction (XRD) were used to support electrochemical results and provide additional evidence on the morphological changes of the N80 steel surface during the corrosion inhibition process. Furthermore, theoretical calculations based on density functional theory (DFT) were employed to correlate the inhibition ability of synthesized benzoxazole derivatives with its quantum chemical parameters.

2. Experimental Section

2.1. Materials

2-aminophenol, polyphosphoric acid, isoquinoline-1-carboxylic acid, 6-hydroxy-2-pyridine carboxylic acid, and salicylic acid were purchased from Macklin reagent (Shanghai, China). Ethanol, ethyl, and magnesium sulfate anhydrous were obtained from Aladdin Reagent (Shanghai, China). All chemicals were used as received without any further purification.

2.2. Synthesis of Corrosion Inhibitors

BOP, BOPO, and QBO were synthesized according to the reported literature [6]. During the experiment process, and the synthetic route is shown in **Figure 1**. Polyphosphoric acid (40 g) was added to a mixture of 2-aminophenol (10 mmol) and the corresponding dicarboxylic acid derivatives (10 mmol) at 60°C. Afterward, these reactants were subjected to a temperature-programmed reaction under nitrogen gas: 1 h at 60°C, 3 h at 120°C, and 4 h at 200°C. The progress of the reaction was monitored by Thin Layer Chromatography. The mixture was

quenched with ice water and then extracted with ethyl acetate. The organic layer was dried by anhydrous magnesium sulfate and evaporated to give the crude product. Finally, the pure product (BOP, BOPO, and QBO) were obtained by which was purified by crystallization with ethanol ether. Moreover, $^1\text{H-NMR}$ and FT-IR spectra confirmed the formation of corrosion inhibitors, showing in **Figure 2** and **Figure 3**.

2.3. Electrochemical Measurements

Potentiodynamic polarization and electrochemical impedance measurement were carried out at the Chi760e electrochemical workstation with a classical three-electrode system at 303 K controlled in the thermostat water bath. N80 steel

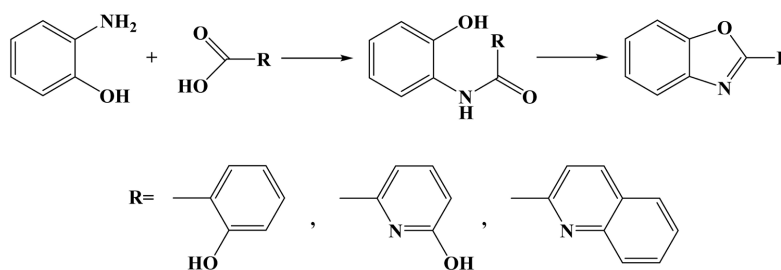


Figure 1. Synthetic route of inhibitors BOP, BOPO, and QBO.

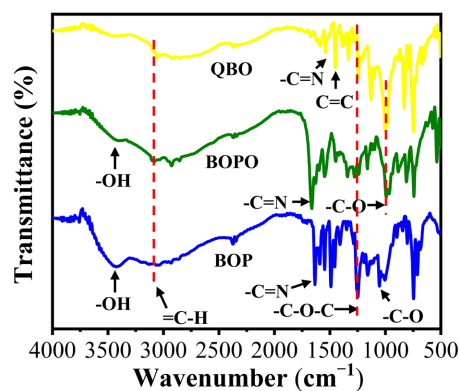
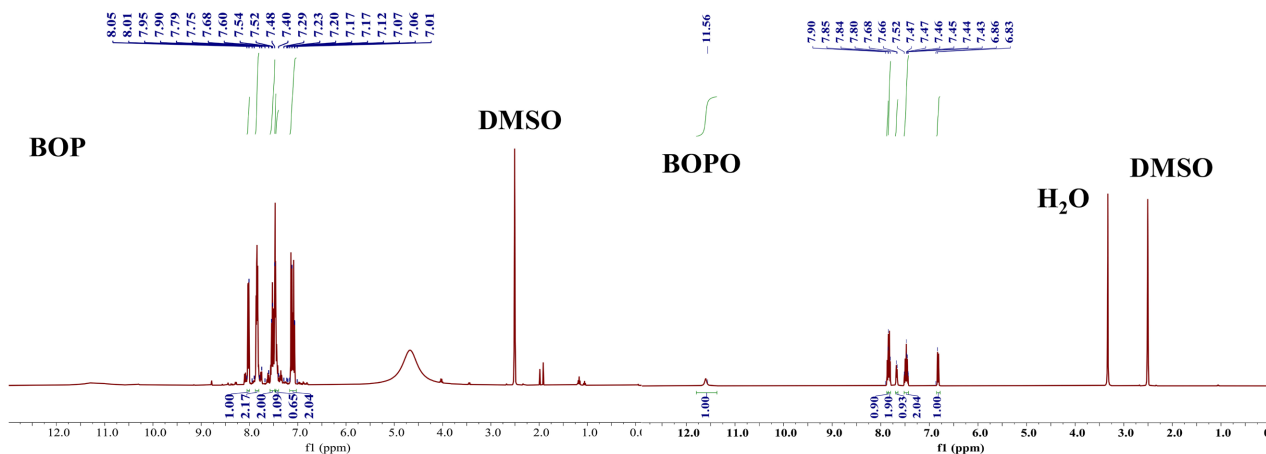


Figure 2. The FT-IR spectra of BOP, BOPO, and QBO.



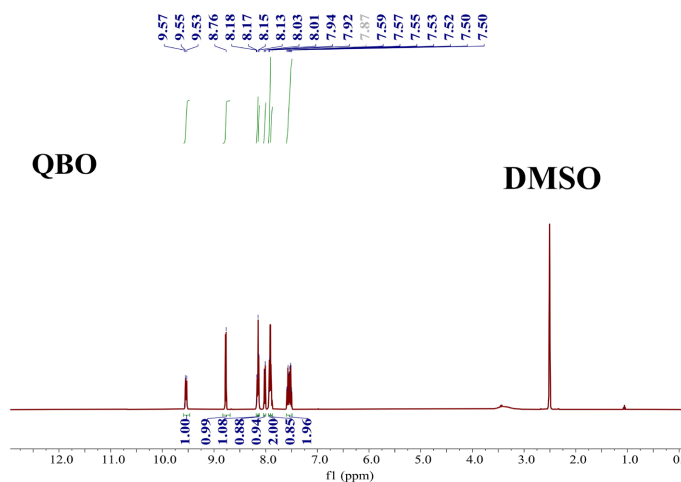


Figure 3. The ¹H-NMR spectra of BOP, BOPO, and QBO.

was used as the working electrode (WE) and polished on 500 to 4000 mesh sandpaper before each measurement. The platinum sheet was applied as the counter electrode (CE), the saturated calomel electrode was selected as a reference electrode (RE) and connected to a Lukin capillary. Before electrochemical tests, the WE was kept in the test solution for 30 min, and then the open circuit potential (OCP) was monitored for 60 min to obtain a steady state. Polarization curves measurements were performed at a constant sweep rate of 1 mV·s⁻¹ in the scanning range from -250 mV to +250 mV, concerning the open circuit potential (OCP). In addition, the corrosion current density was obtained by Tafel extrapolation. The experiments were performed in quiescent conditions while the temperature was maintained constant (within ±1 °C). The average values of three replicates obtained for each test are reported.

2.4. Surface Analyses

FT-IR (Thermo Fisher Scientific, America) technique was used to study the corrosion inhibition on the N80 steel surface after immersion for 24 h in 1 M HCl solution in the spectral range of 500 - 4000 cm⁻¹. The morphologies of the studied N80 steel surfaces in the absence and presence of the investigated corrosion inhibitors were recorded by using FE-SEM (TESCAN, Czech Republic) at 10.0 kV. In addition, the XRD patterns of the samples were investigated by X-ray diffraction (XRD, PALMERNACO) from 20° to 90° at a scan rate of 10°/min.

2.5. Quantum Chemical Calculation

DTF was performed to optimize the geometries of inhibitors molecules using the Dmol³ module in Material Studio 2017 software [7]. The B3LYP was used for the electronic exchange-correlation potential, and all electronic calculations were performed with double numeric quality with polarization (DNP) basis set [8] [9]. In addition, the solvent (water) model was involved in all calculations [10]. A Fermi smearing of 0.005 Ha and a real space cutoff of 3.7 Å was used to im-

prove the computational performance [11]. The convergence criteria of energy, displacement, and gradient were 1×10^{-5} Ha, 5×10^{-3} Å, and 2×10^{-3} Ha/Å, respectively [12] [13].

To explain the interactions between their inhibitors and the metal surface, a set of electronic properties such as the energy of the highest occupied molecular orbital (E_{HOMO}), the energy of the lowest unoccupied molecular orbital (E_{LUMO}), electron affinity (A), ionization potential (I), energy gap (ΔE), global hardness (η) were calculated at the same level of theory. Following Koopmans' theorem, the electronic parameters were calculated by the following equation [14] [15] [16] [17]:

$$I = -E_{\text{HOMO}} \quad (1)$$

$$A = -E_{\text{LUMO}} \quad (2)$$

$$\chi = (I + A)/2 \quad (3)$$

$$\eta = (I - A)/2 \quad (4)$$

$$\Delta E = I - A \quad (5)$$

According to these values, the fraction of electrons transferred (ΔN) was computed through the equation:

$$\Delta N = \frac{\chi_{\text{Fe}} - \chi_{\text{inh}}}{2(\eta_{\text{Fe}} + \eta_{\text{inh}})} = \frac{\Phi_{\text{Fe}} - \chi_{\text{inh}}}{2\eta_{\text{inh}}} \quad (6)$$

For the metal surface, the work-function Φ is taken as its electronegativity, whereas the chemical hardness is neglected because η of the bulk metals is related to the inverse of their density of states at the Fermi level, which is an exceedingly small number [18].

3. Results and Discussion

3.1. Characterization of BOP, BOPO, and QBO

Benzoxazole derivatives were characterized by FT-IR, and the results were shown in **Figure 2**. The absorption peak of BOP appears at 3421 cm^{-1} , which can be attributed to -OH stretching vibration. The absorption band at 1631 cm^{-1} is assigned to the C=N bending vibration. The absorption bands at 1282 cm^{-1} and 1049 cm^{-1} are all assigned to the -C-O-C bending vibration [19]. Compared with the infrared absorption peak of BOP, the C=N absorption peak of BOPO shifts slightly to 1661 cm^{-1} due to the presence of pyridyl [20]. The absorption peak of QBO appears at 1585 cm^{-1} , 1537 cm^{-1} , and 1385 cm^{-1} , which can be assigned to the skeleton vibration of the quinoline ring. The absorption band at 1621 cm^{-1} and 1279 cm^{-1} are assigned to the C=N and -C-O-C bending vibration [21]. The appearance of characteristic peaks of these substances indicates that they may be the target product. Moreover, further characterization is made by some parameters such as $^1\text{H-NMR}$ and melting point, as shown in **Figure 3** and **Table 1**. The results show that the synthesized substances are all target products.

Table 1. Characterisation data for BOP, BOPO, and QBO.

Name	Mol. formula (mol.wt)	Yield (%)	M.P. (°C)	¹ HNMR
BOP	C ₁₃ H ₉ NO ₂ (211.22)	90.1	120.0 - 123.4	(400 MHz, DMSO- <i>d</i> ₆) δ 8.02 (d, <i>J</i> = 7.9 Hz, 1H), 7.88 - 7.81 (m, 2H), 7.58 - 7.47 (m, 2H), 7.47 - 7.45 (m, 1H), 7.45 - 7.40 (m, 1H), 7.17 - 7.03 (m, 2H).
BOPO	C ₁₂ H ₈ N ₂ O ₂ (212.20)	93.4	147.6 - 149.8	(400 MHz, DMSO- <i>d</i> ₆) δ 9.54 (d, <i>J</i> = 10.0 Hz, 1H), 8.76 (s, 1H), 8.21 - 8.11 (m, 2H), 8.02 (d, <i>J</i> = 8.0 Hz, 1H), 7.92 (s, 2H), 7.57 - 7.52 (m, 1H).
QBO	C ₁₆ H ₁₀ N ₂ O (246.26)	92.7	190.5 - 193.0	(400 MHz, DMSO- <i>d</i> ₆) δ 9.56 - 9.48 (m, 1H), 8.76 (s, 1H), 8.16 (s, 1H), 8.15 (s, 1H), 8.02 (d, <i>J</i> = 8.0 Hz, 1H), 7.92 (d, <i>J</i> = 7.5 Hz, 2H), 7.90 - 7.86 (m, 1H), 7.61 - 7.48 (m, 2H).

3.2. Electrochemical Experiments

3.2.1. Potentiodynamic Polarization (PDP)

Polarization curves obtained for N80 steel corrosion with and without BOP, BOPO, and QBO are shown in **Figure 4**. Electrochemical corrosion parameters, such as corrosion potential (E_{corr}), cathodic Tafel slopes (β_c), and corrosion current (I_{corr}), are obtained by extrapolation of the Tafel lines. The detail is given in **Table 1**. Corrosion current density is determined from the intercept of the corrosion potential of extrapolated cathodic and anodic Tafel linear region. The inhibition efficiency (IE) is calculated as follow:

$$IE (\%) = \frac{I_{\text{corr}}^0 - I_{\text{corr}}^1}{I_{\text{corr}}^0} \times 100 \quad (7)$$

where I_{corr}^0 and I_{corr}^1 are the values of corrosion current density of uninhibited and inhibited specimens, respectively.

As seen in **Figure 4**, compared with the blank solution, the polarization curves of anode and cathode both move to a lower current direction with the presence of corrosion inhibitors, suggesting that the rate of anodic dissolution and cathodic hydrogen absorption reaction of metal were suppressed. The cathodic polarization curve was linear, suggesting that the cathodic hydrogen absorption reaction is activation-controlled, and the addition of inhibitors does not change the mechanism [22] [23]. Meanwhile, the anodic polarization curve exhibited non-linear behavior. There is an inflection point in each of the anodic curves, indicating some kinetic barrier effect, maybe the deposition of a corrosion product film and then its removal by intensively evolved hydrogen bubbles [24]. Moreover, the rate of these reactions slows down more distinctly with the increase of corrosion inhibitor concentration. In the presence of all the three inhibitors, corrosion potential exhibits a distinct positive displacement concerning that for the uninhibited sample, though the shift is limited to a small extent of around 30 mV. The three inhibitors are mixed-type and the inhibition of anodic metal dissolution is stronger than cathodic hydrogen evolution.

As is shown in **Table 2**, the I_{corr} values decrease in the order of QBO > BOPO > BOP, and hence IE follows the reverse trend. Further, an increase in inhibition concentration leads to a decrease in I_{corr} value. This result is ascribed to

the blocking effect at higher concentrations, thereby blocking the electrochemical reactions on the surface of N80 steel [25].

Table 2. Fitted polarization curves parameters for N80 steel in 1 M HCl solution with different concentrations of BOP, BOPO, and QBO.

Inhibitors	C_{inh} /M	β_c /(mV·dec ⁻¹)	R /(Ω ·cm ²)	I_{corr} /(10 ⁻⁴ A·cm ⁻²)	E_{corr} /V	IE /%
	Blank	8.5	24.1	9.849	-0.489	—
BOP	1×10^{-5}	7.0	36.6	6.867	-0.469	30.28
	5×10^{-5}	8.7	41.6	5.982	-0.471	39.26
	1×10^{-4}	9.2	51.3	4.826	-0.463	51.00
	1×10^{-3}	5.2	60.3	3.985	-0.457	59.54
BOPO	1×10^{-5}	6.4	75.3	3.127	-0.476	68.25
	5×10^{-5}	8.5	92.7	2.857	-0.488	70.99
	1×10^{-4}	5.8	120.5	2.142	-0.491	78.25
	1×10^{-3}	7.2	175.9	1.730	-0.467	82.43
QBO	1×10^{-5}	7.7	124.5	1.928	-0.488	80.42
	5×10^{-5}	7.2	161.8	1.752	-0.467	82.21
	1×10^{-4}	6.5	175.4	1.639	-0.484	83.36
	1×10^{-3}	3.2	187.3	1.555	-0.455	85.21

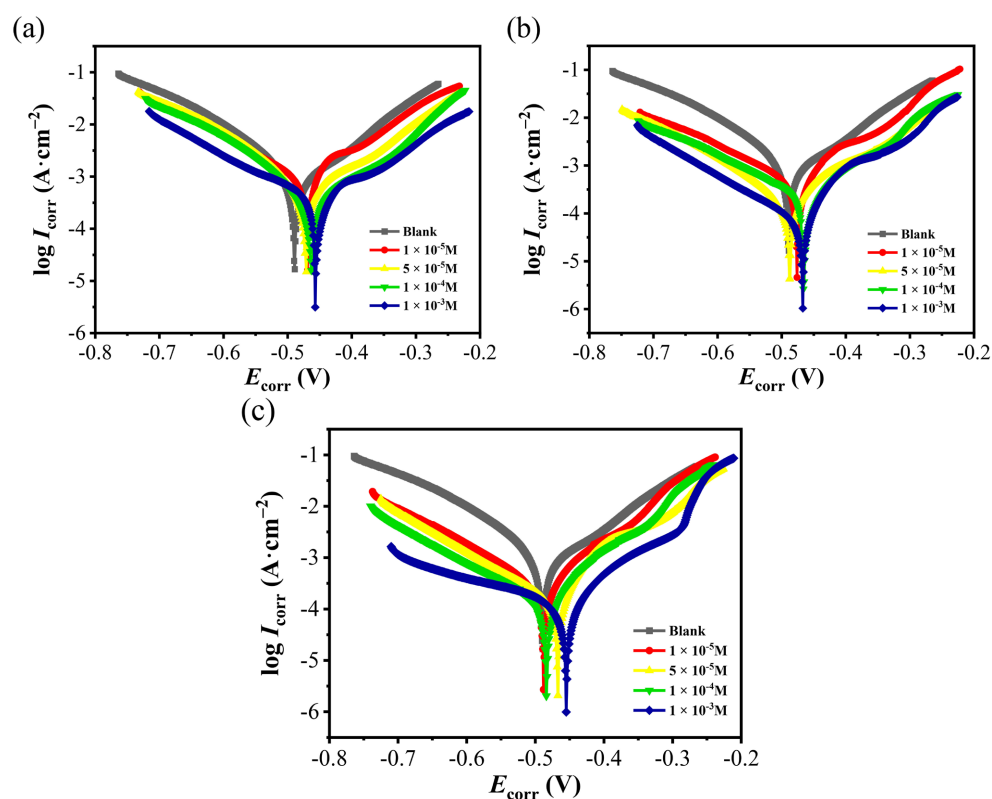


Figure 4. Polarization curves of N80 steel in 1 M HCl solution with various concentrations of inhibitors: (a) BOP; (b) BOPO; (c) QBO.

The observed trend manifests that for a particular substitution position, the corrosion inhibition efficiency of the inhibitor containing multiple benzene rings and heteroatoms is better.

3.2.2. Electrochemical Impedance Spectroscopy

The Nyquist curves of the three inhibitors with the different concentrations in 1M HCl solution are shown in **Figure 5**. Compared to the blank solution, the inhibitors did not alter the shape of the Nyquist curves, which suggests these inhibitors controlled the activity of the corrosion reaction rather than altering the corrosion mechanism [26] [27]. For all the inhibitors, Nyquist curves showed a non-standard semicircle owing to the microscopic roughness of the electrode surface and the adsorption of the inhibitor [28] [29]. Moreover, the diameter of the capacitive loop was seen to increase gradually with concentration. This result suggests that the adsorption degree increases with the concentration of the inhibitors [30].

In **Figure 6**, the inhibitor increased the impedance modulus ($\log|Z|$) compared with blank solution, and the $\log|Z|$ of each inhibitor increased with the inhibitor concentration, which confirms that the corrosion of N80 steel was retarded effectively. Furthermore, all phase angles are lower than 90 degrees, which may be ascribed to the frequency dispersion due to the geometrical factors, such as roughness inhomogeneous of electrode surface [31] [32]. The equivalent

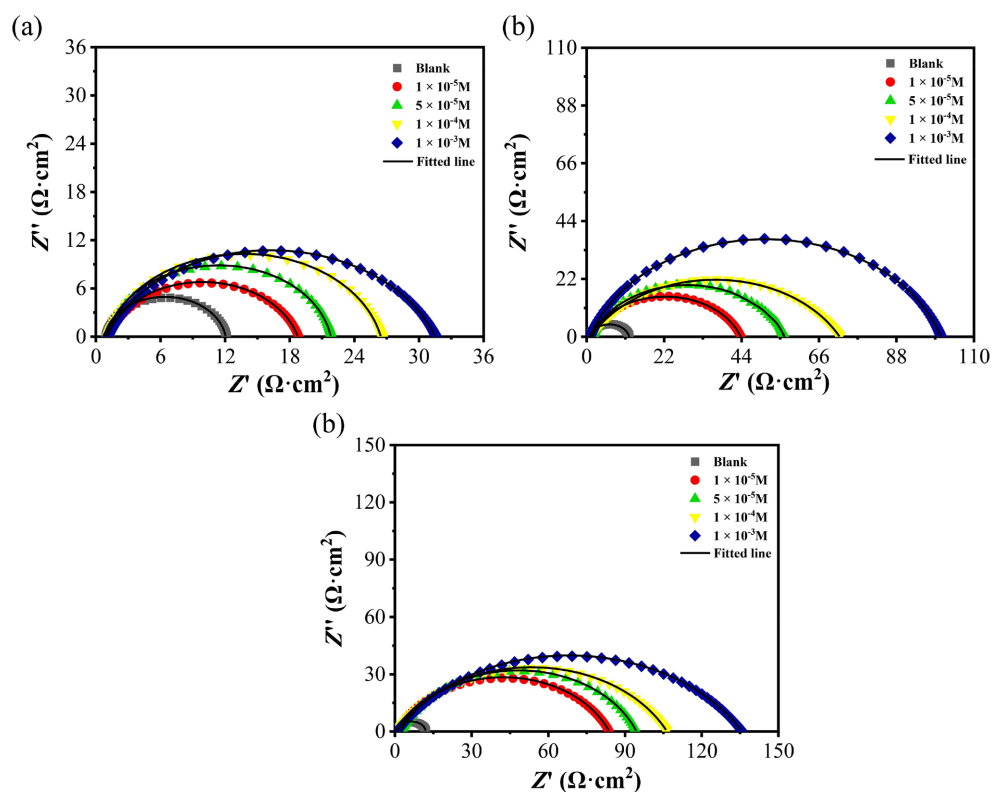


Figure 5. Nyquist plots of N80 steel in 1 M HCl solution with various concentrations of inhibitions: (a) BOP; (b) BOPO; (c) QBO.

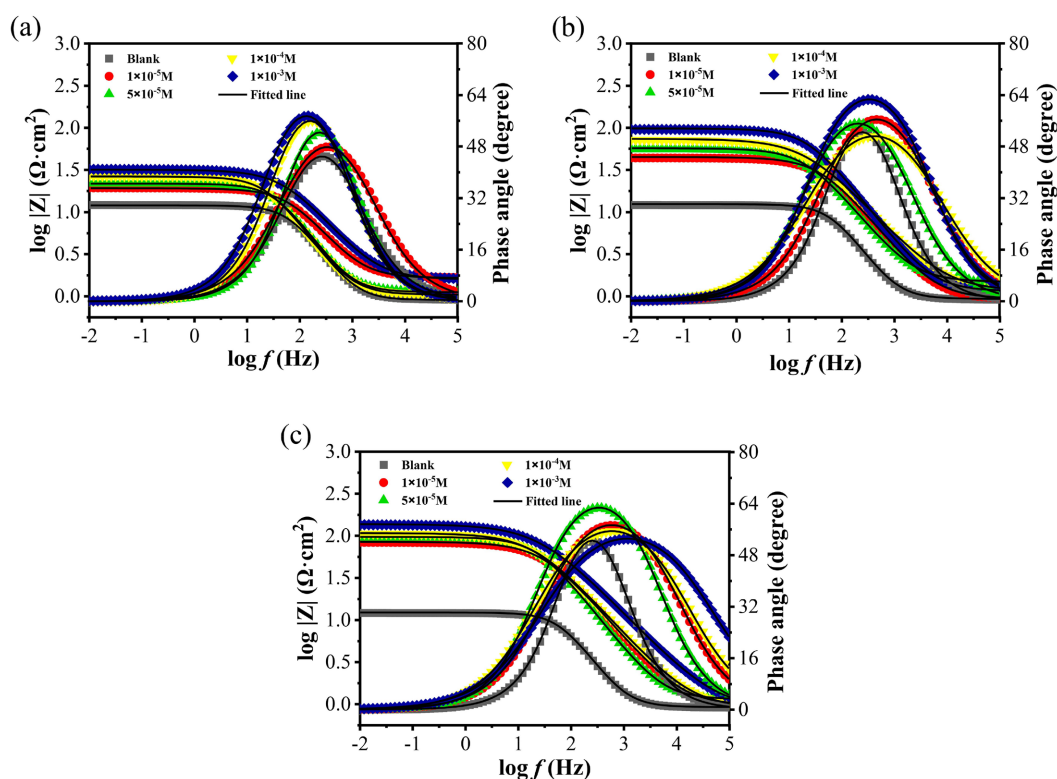


Figure 6. Bode and phase angle plots of N80 steel in 1 M HCl solution with various concentrations of inhibitors: (a) BOP; (b) BOPO; (c) QBO.

circuit proposed to fit the impedance data are shown in **Figure 7**, including a solution resistance (R_s), the charge transfer resistance (R_{ct}), and the constant phase element (CPE). The fitted impedance parameters, such as R_s , R_{ct} , and CPE_{dl} are listed in **Table 3**. The constant phase element (CPE) is related to the double layer capacity (C_{dl}) and its impedance is as follows:

$$Z_{CPE} = Y_0^{-1} (i\omega)^{-n} \quad (8)$$

where Y_0 , i , ω , and n stand for CPE constant, imaginary root, angular frequency, and the deviation indicator. The variable n is connected to the electrode surface homogeneity. To obtain a direct correlation between R_{ct} and C_{dl} , the latter has been recalculated using the following equation:

$$C_{dl} = Y_0^{\frac{1}{n}} R_{ct}^{\frac{1}{n}-1} \quad (9)$$

The IE of the inhibitors are calculated through the following equation:

$$IE(\%) = \frac{R_{ct} - R_{ct}^0}{R_{ct}} \times 100 \quad (10)$$

where R_{ct} and R_{ct}^0 are the values of charge transfer resistance observed in the presence and absence of inhibitor, respectively. At a specific concentration, the order of the inhibition efficiencies is $QBO > BOPO > BOP$. The most significant resistance value for QBO suggests that QBO can most effectively block the cor-

rosion medium's attack. Furthermore, the inhibition efficiency for each inhibitor increases with the increase of concentration and reaches the highest value at 1 mM. As shown in **Table 2**, the addition of inhibitors increased R_{ct} value and decreased C_{dl} value. These results suggest that the water molecules at the metal/solution interface are gradually replaced by the adsorbed organic molecules, resulting in a decrease in the local dielectric constant and the thickening of the electric double layer [33] [34] [35].

3.3. Effects of KI on Corrosion Inhibiting Properties

At present, iodide ions have been examined in detail because of their essential role in improving the inhibition performance of organic compounds during the corrosion inhibition process [36]. When the concentration of the three inhibitors was 1 mM, the effect of KI (10 mM) on the inhibition performance in HCl solution was evaluated in this work. As seen in **Figure 8**, the Nyquist plots show an incomplete semicircle, indicating that a charge transfer process always controls N80 steel corrosion. Therefore, the addition of KI does not alter the corrosion mechanism of the N80 steel.

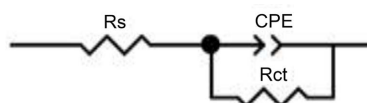


Figure 7. The equivalent circuit fitting the EIS data.

Table 3. Fitted EIS parameters for N80 steel in 1 M HCl solution with different concentrations of BOP, BOPO, and QBO.

Inhibitor	C_{inh} /M	R_s / $(\Omega \cdot \text{cm}^2)$	CPE_{dl}		C_{dl} / $(\mu\text{F} \cdot \text{cm}^{-2})$	R_{ct} / $(\Omega \cdot \text{cm}^{-2})$	IE /%
			$Y_0 \times 10^{-5}$ / $(\text{S} \cdot \text{s}^n \cdot \text{cm}^{-2})$	n			
	Blank	0.902	40.122	0.807	227.93	11.23	—
BOP	1×10^{-5}	1.666	39.890	0.856	120.21	17.66	36.41
	5×10^{-5}	1.128	32.152	0.861	91.89	20.79	45.98
	1×10^{-4}	1.054	30.854	0.869	84.34	25.57	56.08
	1×10^{-3}	1.594	27.075	0.876	70.06	30.50	63.18
BOPO	1×10^{-5}	0.916	36.391	0.872	107.11	42.94	73.85
	5×10^{-5}	1.448	31.218	0.877	88.56	54.23	79.29
	1×10^{-4}	1.122	26.965	0.873	80.94	70.88	84.16
	1×10^{-3}	1.121	23.426	0.854	87.46	94.76	88.15
QBO	1×10^{-5}	0.948	28.461	0.889	75.05	82.87	86.45
	5×10^{-5}	1.121	24.426	0.874	74.63	94.76	88.15
	1×10^{-4}	0.879	23.686	0.876	71.69	105.50	89.36
	1×10^{-3}	0.846	17.381	0.873	53.75	134.90	91.67

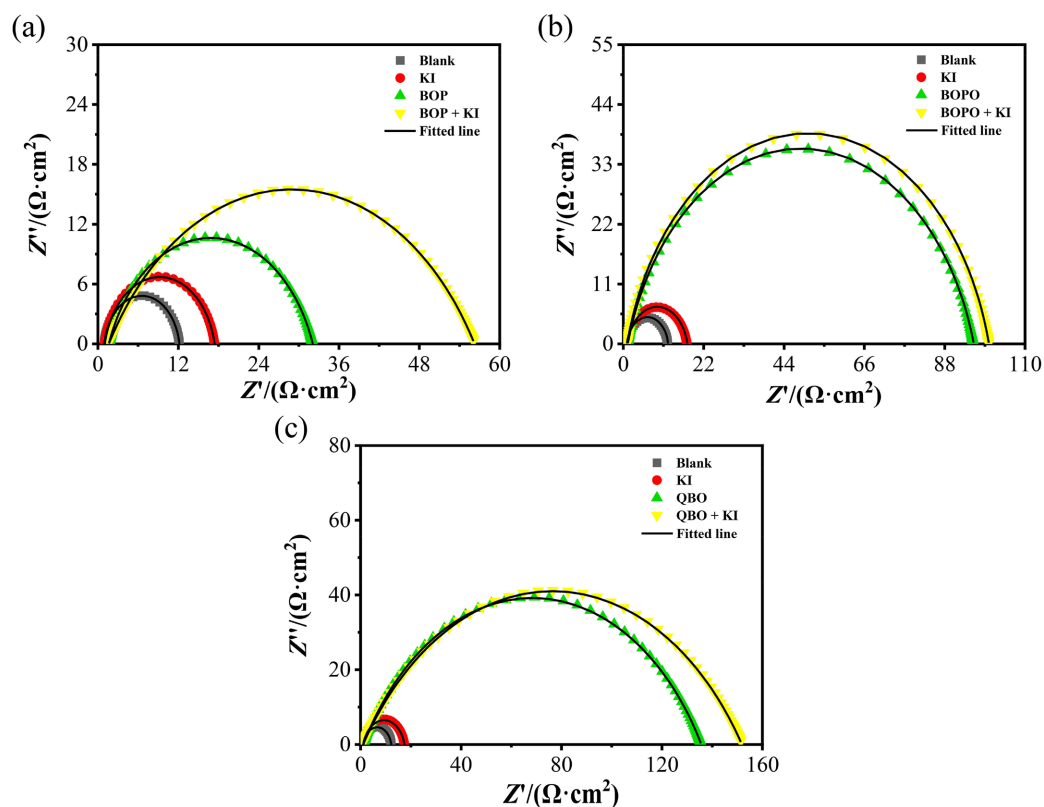


Figure 8. Nyquist plots of N80 steel in 1 mol·L⁻¹ HCl solution in the presence and the absence of 10 mmol·L⁻¹ KI and 1 mmol·L⁻¹ inhibitors: (a) BOP; (b) BOPO; (c) QBO.

Moreover, from this graph, we find that the capacitive loop's diameter, with the presence of both inhibitors and KI, is significantly increased compared to BOP, BOPO, and QBO alone, reflecting the enhanced protective capacity of studied inhibitors in the presence of iodide ions. The electrochemical parameters derived from Nyquist plots are shown in **Table 4**. The R_{ct} values increased after adding KI compared with those without KI. Correspondingly, for the combined system (inhibitors + KI), the C_{dl} values decrease compared to the system without KI. To investigate the interactive relationship between inhibitors and KI, the synergistic parameter (S) was calculated using the equation suggested by Aramaki and Hackerman [37] [38] [39]:

$$S = \frac{1 - (\theta_1 + \theta_2) + \theta_1\theta_2}{1 - \theta_{1+2}} \quad (11)$$

wherein, θ_1 and θ_2 are the surface coverage values calculated with the presence of KI and Inhibitors, respectively. θ_{1+2} is the surface coverage values of inhibitor-KI mixtures (KI + Inhibitor). $S > 1$ indicates the synergistic behavior of a selected inhibitor combination, and $S < 1$ indicates the competitive adsorption of a selected inhibitor combination [40]. From **Table 4**, the S of BOP/KI compound inhibitor is higher than 1, which can be attributed to improved adsorption of BOP, indicating the synergistic effect. However, the S of BOPO/KI and QBO/KI compound inhibitors are less than 1. This result demonstrates that the interac-

tion relationship between inhibitors and KI molecule is competitive adsorption, not synergistic inhibition. To confirm the EIS analyses, the polarization experiment was also conducted. The polarization curves are shown in **Figure 9**, while electrochemical corrosion parameters for each system are summarized in **Table 4**. The results show that KI/inhibitor systems had the highest inhibition efficiency value than systems inhibited using inhibitors alone. The results are consistent with those calculated from EIS.

3.4. Adsorption Isotherms

The adsorption of inhibitors on the metal surface can be analyzed using the adsorption isotherm [4]. The degree of surface coverage (θ) at different concentrations (**Table 3**) calculated is as follow:

$$\theta = IE(\%)/100 \quad (12)$$

The θ values obtained from EIS measurement were used to fit different adsorption isotherms such as Langmuir, Temkin, and Frumkin (**Figure 10**). It is found that among the previously mentioned adsorption isotherm, Langmuir adsorption isotherm fitted well with regression coefficient (R^2) close to 1. This result shows that the adsorption of organic molecules on the metal surface is monolayer [41].

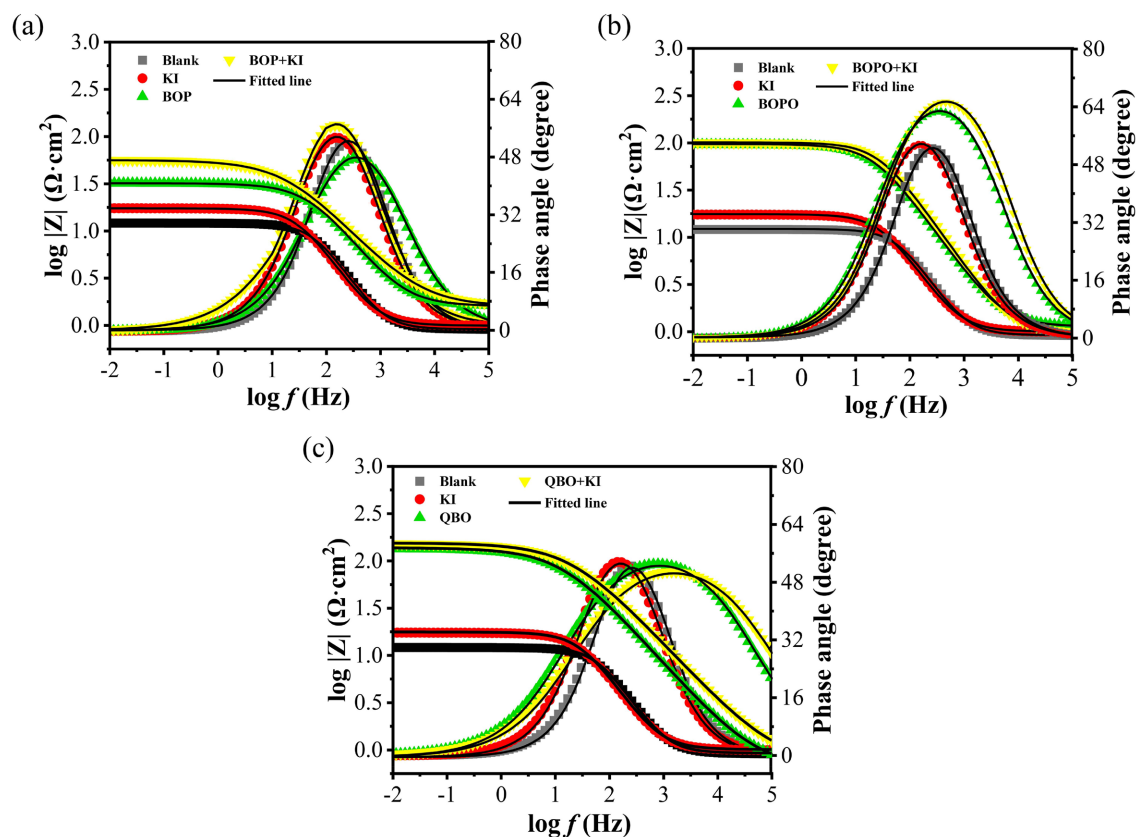


Figure 9. Bode and phase angle plots of N80 steel in 1 mol·L⁻¹ HCl solution in the presence and the absence of 10 mmol·L⁻¹ KI and 1 mmol·L⁻¹ inhibitors: (a) BOP; (b) BOPO; (c) QBO.

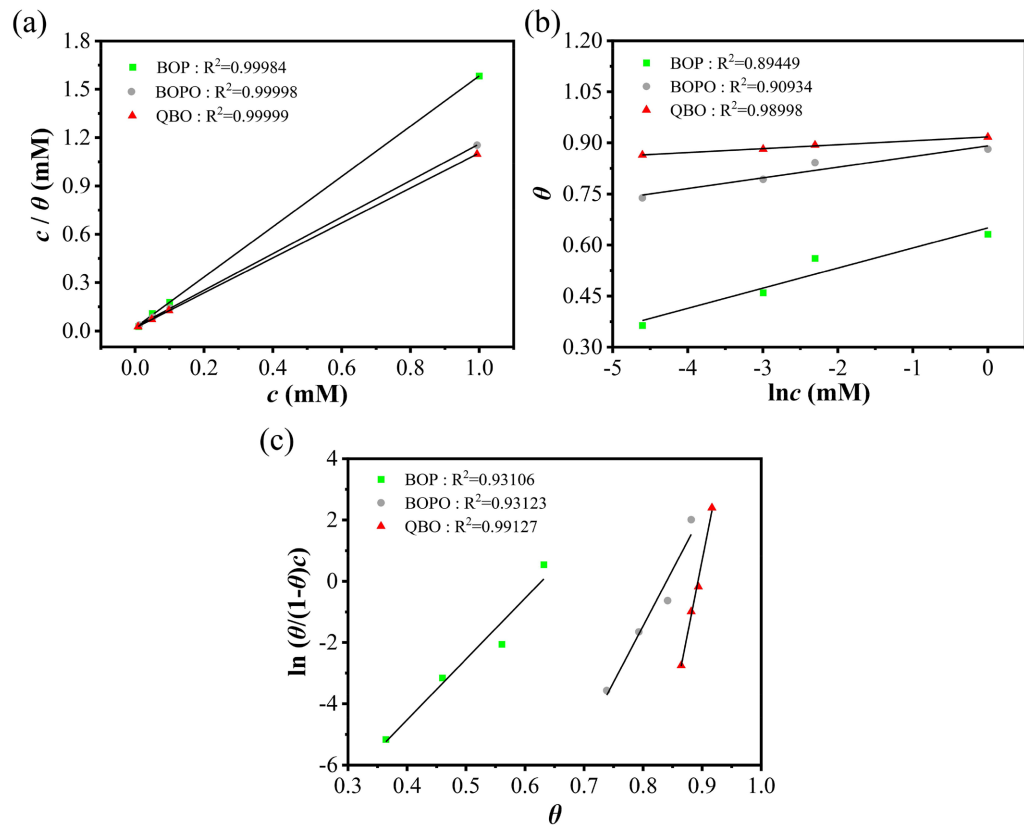


Figure 10. Adsorption isotherm for compounds BOP, BOPO, and QBO on N80 steel in 1 M HCl solution (a) Langmuir, (b) Temkin and (c) Frumkin.

Table 4. Fitted EIS and Polarization curves parameters for N80 steel in 1 M HCl solution containing KI alone (10 mM) and with 1 mM BOP.

Inhibitor	EIS method						
	R_s $\backslash(\Omega \cdot \text{cm}^{-2})$	$Y_0 \times 10^{-5}$ $\backslash(\text{S} \cdot \text{s}^{-1} \cdot \text{cm}^{-2})$	n	C_{dl} $\backslash(\mu\text{F} \cdot \text{cm}^{-2})$	R_{ct} $\backslash(\Omega \cdot \text{cm}^{-2})$	IE /%	S
Blank	0.902	40.122	0.807	173.00	11.23	—	—
KI	0.993	30.814	0.811	131.48	16.41	31.57	—
BOP + KI	1.578	24.757	0.879	66.80	54.68	79.46	1.23
BOPO + KI	0.966	18.592	0.875	54.42	99.06	88.66	0.72
QBO + KI	0.704	12.034	0.859	41.26	151.30	92.5 8	0.77
Inhibitor	PDP method						
	β_c $\backslash(\text{mV} \cdot \text{dec}^{-1})$	R $\backslash(\Omega \cdot \text{cm}^{-2})$	I_{corr} $\backslash(10^{-4} \text{A} \cdot \text{cm}^{-2})$	E_{corr} /V	IE /%	S	
Blank	8.500	24.1	9.849	-0.489	—	—	
KI	9.192	38.9	7.248	-0.495	26.41	—	
BOP + KI	5.855	100.4	2.635	-0.470	73.25	1.11	
BOPO + KI	6.459	182.6	1.633	-0.464	83.42	0.78	
QBO + KI	3.061	207.4	1.347	-0.458	86.32	0.80	

The Langmuir adsorption isotherm is as follows:

$$\text{Langmuir: } \frac{c}{\theta} = \frac{1}{K_{\text{ads}}} + c \quad (13)$$

where K_{ads} is the adsorption equilibrium constant, and c is the inhibitor concentration. The K_{ads} was linked to the energy of adsorption (ΔG_{ads}) using the relation [42]:

$$\Delta G_{\text{ads}} = -RT \ln(55.5K_{\text{ads}}) \quad (14)$$

where R is the gas constant, T is the temperature, and 55.5 is the molar concentration of water in solution. The calculated ΔG_{ads} values of the synthesized inhibitor molecules are given in **Table 5**. The obtained negative value of ΔG_{ads} indicates that the adsorption of the three inhibitors on N80 steel surfaces is spontaneous. It is well known that the values of ΔG_{ads} around $-20 \text{ kJ}\cdot\text{mol}^{-1}$ or lower are consistent with the electrostatic interaction (physisorption). Those of the order of $-40 \text{ kJ}\cdot\text{mol}^{-1}$ or higher are associated with chemisorption [43] [44]. The obtained ΔG_{ads} values for BOP is $-37.21 \text{ kJ}\cdot\text{mol}^{-1}$, reflecting the mixed types of adsorption (both physisorption and chemisorption) taking place on the metallic surfaces. Moreover, chemisorption is predominating over physisorption. The obtained ΔG_{ads} values for BOPO and QBO are $-40.96 \text{ kJ}\cdot\text{mol}^{-1}$ and $-43.24 \text{ kJ}\cdot\text{mol}^{-1}$, respectively, reflecting the chemisorption taking place on the metallic surfaces.

3.5. Surface Analyses

3.5.1. FT-IR Analysis

FT-IR spectra further analyzed the adsorption mechanism of the three inhibitors on the N80 steel surface, and the result is shown in **Figure 11**. In blank solution, the broad peak at 3424 cm^{-1} signified the -OH stretching vibration due to the formation of FeOOH [45] [46]. The water bending bands are observed at 1629 cm^{-1} , assigned to the OH vibrations [47]. The absorption bands at 1058 cm^{-1} are assigned to the surface's -OH bending vibration [48]. With the addition of BOP, BOPO, and QBO, the absorption peak of 3424 cm^{-1} gradually becomes weaker, indicates that the addition of inhibitors inhibits the process of Fe to FeOOH. With the addition of the inhibitors, the absorption peak of 1058 cm^{-1} gradually becomes weaker with some deviation. Since the characteristic peak C=N of the corrosion inhibitor is similar to the absorption peak at 1629 cm^{-1} , it is impossible to determine the functional group corresponding to the absorption peak here. In contrast with **Figure 1**, some absorption peaks present in pure compound appear in the adsorption layer on the N80 steel surface, which means that most of the functional groups of the three inhibitors are present in the adsorbed surface film. Moreover, some of the peaks for the pure compound have diminished or even vanished, suggests that these functional groups are directly involved in inhibitors inhibition, thus confirming the proposed adsorption of the inhibitors on the N80 steel [49] [50].

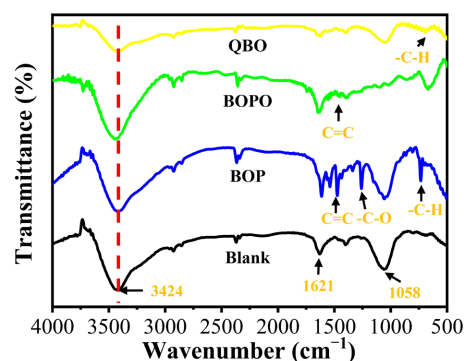


Figure 11. FT-IR spectra of corrosion products of N80 steel soaked for 24 h in 1 mol·L⁻¹ HCl solution without corrosion inhibitor or containing 1 mmol·L⁻¹ BOP, BOPO and QBO.

Table 5. Adsorption equilibrium constants (K_{ads}) and ΔG_{ads}^0 of compounds BOP, BOPO, and QBO on N80 steel in 1 M HCl solution.

Inhibitors	R^2	Slope	K_{ads}	ΔG_{ads}^0 (kJ/mol)
BOP	0.99984	1.56182	46,728.97	-37.21
BOPO	0.99998	1.12976	207,039.34	-40.96
QBO	0.99999	1.08903	512,820.51	-43.24

3.5.2. FE-SEM Analysis

FE-SEM was used to observe the protective effect of an inhibitor directly. The surface morphologies of the N80 steel surface after being immersed in 1 M HCl solution in the presence and absence of 1 mM inhibitors (BOP, BOPO, and QBO) are shown in **Figure 12**. The surface of N80 steel has been severely corroded in the absence of inhibitors. The traces left by sandpaper grinding have been corroded, pits of varying depths appear, and many corrosion products adhere to the surface of the steel sheet. Compared with the blank solution, in the presence of corrosion inhibitors BOP and BOPO, the corrosion on the surface of N80 steel is not so severe, but the surface is still uneven, and at the same time, the surface of the steel sheet still adheres to corrosion products. These results indicate that the protective film formed by these two corrosion inhibitors on the surface of N80 steel is not stable and dense, and the corrosive medium can still contact the surface of N80 steel, resulting in surface corrosion. Among BOP and BOPO, the presence of the latter as corrosion inhibitor shows more robust protective performance. In the presence of corrosion inhibitor QBO, the surface of N80 steel is smooth, and the polishing traces can be observed, indicating that corrosion inhibitor forms a dense protective film on the surface of N80 steel, which effectively protects N80 steel. In conclusion, the protective effects of inhibitors increase in the order of BOP < BOPO < QBO.

3.5.3. XRD Analysis

Figure 13 presents the XRD patterns of the studied N80 steel immersed in 1M HCl solution in the absence and presence of the studied inhibitors BOP, BOPO,

and QBO. Each XRD pattern shows three peaks at 44.64° , 65.02° , and 82.29° , corresponding to the characteristic signals of Fe, FeOOH, and Fe_3O_4 , respectively [50]. This result suggests corrosion inhibition occurred when N80 steel was immersed in 1M HCl solution in the presence and the absence of BOP, BOPO, and QBO [51]. At the peak of 82.29° , the weakening of the peak intensity indicates that the protective film formed by the corrosion inhibitor adsorbed on the surface of the N80 steel inhibits the oxidation process of Fe to Fe_3O_4 . In addition, the lower peak intensity of QBO at 82.29° explains better inhibition performance of QBO than that of BOP and BOPO.

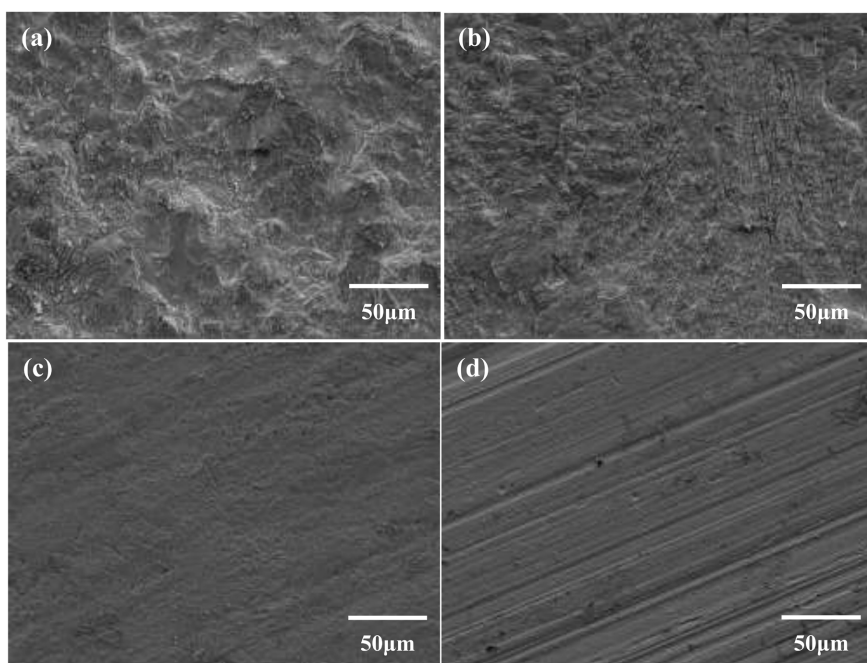


Figure 12. FE-SEM images of the surface of N80 steel soaked for 24 h in 1 mol·L⁻¹ HCl solution without corrosion inhibitor (a), or containing 1 mmol·L⁻¹ BOP (b), BOPO (c) and QBO (d).

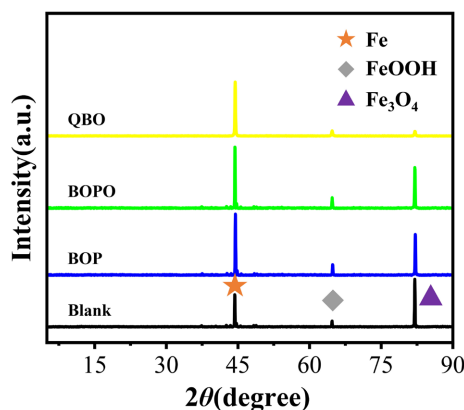


Figure 13. XRD patterns of corrosion products of N80 steel soaked for 24 h in 1 mol·L⁻¹ HCl solution without corrosion inhibitor or containing 1 mmol·L⁻¹ BOP, BOPO and QBO.

3.6. Quantum Chemical Calculations

The experimental results show that three corrosion inhibitors can be adsorbed on the surface of steel and play the important role of anti-corrosion. In this work, quantum chemical calculations were used to study further the relationship between the molecular structure and corrosion inhibition performance [52] [53]. **Figure 14.** shown the frontiers orbitals of BOP, BOPO, and QBO in their optimized form. The HOMO and LUMO of BOP and BOPO are delocalized on the whole molecule, proving that the whole molecular plane is the active center of the reaction. However, the LUMO of QBO is mainly delocalized on the quinoline ring, indicating a preference for accepting electrons. The quantum chemical parameters for all inhibitors are listed in **Table 6.** E_{HOMO} is related to the electron donation capability of the respective molecule. The higher the E_{HOMO} value, the stronger the inhibitor's electron-donating capability and the better inhibition efficiency. E_{LUMO} indicates concerned molecules' ability to accept electrons from the metallic surface. Therefore lower the E_{LUMO} value, the better will be its inhibition efficiency [54]. The ΔE is an essential parameter as a function of reactivity of the inhibitor molecule towards the adsorption on the metallic surface. As ΔE decreases, the molecule's reactivity increases, leading to an increase in the strength of adsorption and hence in the inhibition efficiency [9]. Moreover, the values of E_{LUMO} of the three inhibitions show a decrease in the order of BOP > BOPO > QBO, and ΔE shows a decrease in the order of BOP > BOPO > QBO, suggesting the most substantial ability of QBO to form coordinate bonds with d-orbitals of metal through donating and accepting electrons, which is in good agreement with the experimental results. These results predict that corrosion inhibitors for quinoline substituents should be chemisorbed more effectively and have a better performance than pyridine and benzene substituents. On the other hand, electronegativity (χ) represents the electron attracting capability of the molecule. The higher the electronegativity, the stronger is the attracting power to accept an electron from the metallic surface [15]. Therefore, those inhibitor molecules with higher electronegativity would have strong interaction with the metal surface, and higher inhibition efficiency is observed. From **Table 6,** it is observed that the electronegativity of the three inhibitor molecules follows the trend BOP > BOPO > QBO. Therefore, it is confirmed that corrosion inhibitor for quinoline substituents has the highest ability to accept electrons among the three inhibitor molecules, and these results are in good agreement with the E_{LUMO} trend. Generally, ΔN is a measure of the electron transfer between molecule and metal. If $\Delta N < 3.6$, the inhibition efficiency increases with electrons donation to the metal surface [55]. The calculated ΔN values for the three inhibitions are less than 3.6. Moreover, ΔN gradually increases in the order: BOP < BOPO < QBO. Thus, the extent of bond formation between the inhibitor molecule and the metal surface also follows the same trend, which ultimately dictates the corrosion inhibition potentiality.

In a word, the result obtained through quantum chemical calculation agrees

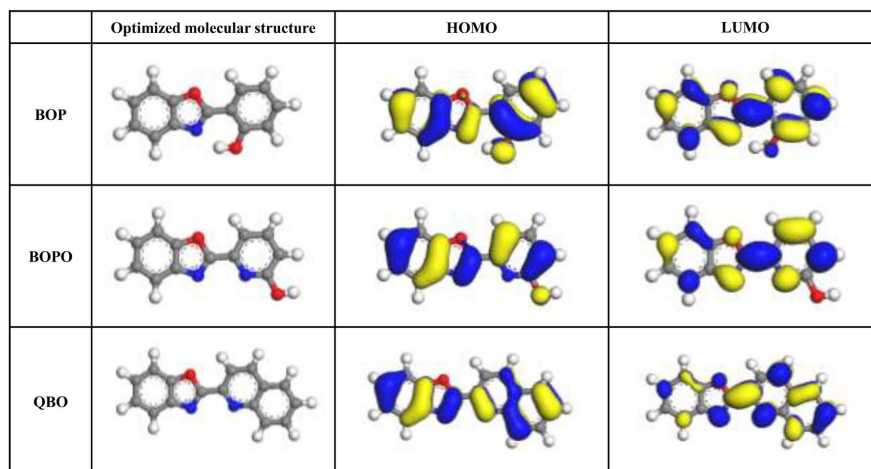


Figure 14. Optimized structures and the frontier molecular orbital density distributions (HOMO and LUMO) were obtained by the B3LYP method with a DNP basis set for BOP, BOPO, and QBO molecules.

Table 6. Quantum chemical parameters were calculated using the B3LYP method with a DNP basis set for BOP, BOPO, and QBO molecules.

Inhibitors	E_{HOMO} /eV	E_{LUMO} /eV	ΔE /ev	χ /eV	η □eV	ΔN
BOP	-6.33	-1.87	4.46	4.10	2.23	3.23
BOPO	-6.52	-2.16	4.37	4.34	2.18	2.90
QBO	-6.51	-2.40	4.11	4.46	2.05	2.61

with the experimental results. The inhibition efficiency of three corrosion inhibitors gradually increases in the order: BOP < BOPO < QBO. That is to say, when the same benzoxazole unit is contained, the nature of the substituent determines the corrosion inhibition efficiency. Inhibition efficiency follows the order: benzene < pyridine < quinoline.

4. Conclusions

- 1) The FT-IR and ¹HNMR results demonstrate that the three target compounds had been synthesized successfully.
- 2) The inhibition efficiency of benzoxazole derivatives in a 1 M HCl solution at 303 K was evaluated by electrochemical experiments, including electrochemical impedance spectroscopy and potentiodynamic polarization. The data of the electrochemical experiments indicate that the inhibition efficiency increases with increasing inhibitor concentration.
- 3) The effect of KI on inhibition efficiency is as follows: BOP and KI are synergistic, BOPO and QBO are competitive adsorptions with KI.
- 4) Surface analyses including FT-IR, FE-SEM, and XRD confirmed the protective effect of these inhibitors.
- 5) Quantum chemical parameters, including the front orbital distribution and the global and local reactivity parameters, such as E_{HOMO} , E_{LUMO} , energy gap

(ΔE), global hardness (η), and electrons transferred (ΔN), demonstrate the inhibition efficiencies obtained from experimental results.

Acknowledgements

This work is supported by State Key Laboratory of Separation Membranes and Membrane Processes (Tiangong University, No. M202109), and the National Natural Science Foundation of China (grant no. 21403017, 21873075).

Conflicts of Interest

The authors declare no conflicts of interest regarding the publication of this paper.

References

- [1] National Research Council (2009) Assessment of Corrosion Education. National Academies Press, Washington DC.
- [2] Su, H., Wang, L., Wu, Y., Zhang, Y. and Zhang, J. (2020) Insight into Inhibition Behavior of Novel Ionic Liquids for Magnesium Alloy in NaCl Solution: Experimental and Theoretical Investigation. *Corrosion Science*, **165**, Article ID: 108410. <https://doi.org/10.1016/j.corsci.2019.108410>
- [3] Onyeachu, I.B., Obot, I.B., Sorour, A.A. and Abdul-Rashid, M.I. (2019) Green Corrosion Inhibitor for Oilfield Application I: Electrochemical Assessment of 2-(2-Pyridyl) Benzimidazole for API X60 Steel under Sweet Environment in NACE brine ID196. *Corrosion Science*, **150**, 183-193. <https://doi.org/10.1016/j.corsci.2019.02.010>
- [4] Liao, L.L., Mo, S., Luo, H.Q., Feng, Y.J., Yin, H.Y. and Li, N.B. (2017) Relationship between Inhibition Performance of Melamine Derivatives and Molecular Structure for Mild Steel in Acid Solution. *Corrosion Science*, **124**, 167-177. <https://doi.org/10.1016/j.corsci.2017.05.020>
- [5] Machnikova, E., Whitmire, K.H. and Hackerman, N. (2008) Corrosion Inhibition of Carbon Steel in Hydrochloric Acid by Furan Derivatives. *Electrochimica Acta*, **53**, 6024-6032. <https://doi.org/10.1016/j.electacta.2008.03.021>
- [6] Um, S.-I. (2007) The Synthesis and Properties of Benzoxazole Fluorescent Brighteners for Application to Polyester Fibers. *Dyes and Pigments*, **75**, 185-188. <https://doi.org/10.1016/j.dyepig.2006.04.024>
- [7] Lgaz, H., Saha, S.K., Chaouiki, A., Subrahmanya Bhat, K., Salghi, R., Shubhalaxmi, *et al.* (2020) Exploring the Potential Role of Pyrazoline Derivatives in Corrosion Inhibition of Mild Steel in Hydrochloric Acid Solution: Insights from Experimental and Computational Studies. *Construction and Building Materials*, **233**, Article ID: 117320. <https://doi.org/10.1016/j.conbuildmat.2019.117320>
- [8] Kovačević, N. and Kokalj, A. (2011) DFT Study of Interaction of Azoles with Cu (111) and Al (111) Surfaces: Role of Azole Nitrogen Atoms and Dipole-Dipole Interactions. *The Journal of Physical Chemistry C*, **115**, 24189-24197. <https://doi.org/10.1021/jp207076w>
- [9] Obot, I., Macdonald, D. and Gasem, Z. (2015) Density Functional Theory (DFT) as a Powerful Tool for Designing New Organic Corrosion Inhibitors. Part 1: An Overview. *Corrosion Science*, **99**, 1-30. <https://doi.org/10.1016/j.corsci.2015.01.037>
- [10] Tan, J., Guo, L., Yang, H., Zhang, F. and El Bakri, Y. (2020) Synergistic Effect of

- Potassium Iodide and Sodium Dodecyl sulfonate on the Corrosion Inhibition of Carbon Steel in HCl Medium: A Combined Experimental and Theoretical Investigation. *RSC Advances*, **10**, 15163-15170. <https://doi.org/10.1039/D0RA02011G>
- [11] Wang, H., Hao, Y., Chen, S., Cheng, M., Li, C., Sun, S., *et al.* (2018) DFT Study of Imidazoles Adsorption on the Grain Boundary of Cu (100) Surface. *Corrosion Science*, **137**, 33-42. <https://doi.org/10.1016/j.corsci.2018.03.009>
- [12] Khaled, K. (2011) Modeling Corrosion Inhibition of Iron in Acid Medium by Genetic Function Approximation Method: A QSAR Model. *Corrosion Science*, **53**, 3457-3465. <https://doi.org/10.1016/j.corsci.2011.01.035>
- [13] Tang, Y., Zhang, F., Hu, S., Cao, Z., Wu, Z. and Jing, W. (2013) Novel Benzimidazole Derivatives as Corrosion Inhibitors of Mild Steel in the Acidic Media. Part I: Gravimetric, Electrochemical, SEM and XPS Studies. *Corrosion Science*, **74**, 271-282. <https://doi.org/10.1016/j.corsci.2013.04.053>
- [14] Dutta, A., Panja, S.S., Nandi, M. and Sukul, D. (2015) Effect of Optimized Structure and Electronic Properties of Some Benzimidazole Derivatives on Corrosion Inhibition of Mild Steel in Hydrochloric Acid Medium: Electrochemical and Theoretical Studies. *Journal of Chemical Sciences*, **127**, 921-929. <https://doi.org/10.1007/s12039-015-0850-x>
- [15] Saha, S.K., Dutta, A., Ghosh, P., Sukul, D. and Banerjee, P. (2015) Adsorption and Corrosion Inhibition Effect of Schiff Base Molecules on the Mild Steel Surface in 1 M HCl Medium: A Combined Experimental and Theoretical Approach. *Physical Chemistry Chemical Physics*, **17**, 5679-5690. <https://doi.org/10.1039/C4CP05614K>
- [16] Yilmaz, N., Fitoz, A. and Emregül, K.C. (2016) A Combined Electrochemical and Theoretical Study into the Effect of 2-((thiazole-2-ylimino) methyl) Phenol as a Corrosion Inhibitor for Mild Steel in a Highly Acidic Environment. *Corrosion Science*, **111**, 110-120. <https://doi.org/10.1016/j.corsci.2016.05.002>
- [17] Kaya, S., Kaya, C., Guo, L., Kandemirli, F., Tüzün, B., Uğurlu, İ., *et al.* (2016) Quantum Chemical and Molecular Dynamics Simulation Studies on Inhibition Performances of Some Thiazole and Thiadiazole Derivatives against Corrosion of Iron. *Journal of Molecular Liquids*, **219**, 497-504. <https://doi.org/10.1016/j.molliq.2016.03.042>
- [18] Guo, L., El Bakri, Y., Tan, J., Anouar, E.H., Kaya, S. and El Mokhtar, E. (2019) Multidimensional Insights Involving Electrochemical and *in Silico* investigation into the Corrosion Inhibition of Newly Synthesized Pyrazolotriazole Derivatives on Carbon Steel in a HCl Solution. *RSC Advances*, **9**, 34761-34771. <https://doi.org/10.1039/C9RA05881H>
- [19] Arshad, M. (2018) Synthesis, Characterization, and Antimicrobial Assessment of Some Computationally Bioactive 1, 2-Oxazole Derivatives. *Russian Journal of General Chemistry*, **88**, 1886-1891. <https://doi.org/10.1134/S1070363218090207>
- [20] Brycki, B., Małecka, I., Koziróg, A. and Otlewska, A. (2017) Synthesis, Structure and Antimicrobial Properties of Novel Benzalkonium Chloride Analogues with Pyridine Rings. *Molecules*, **22**, Article No. 30. <https://doi.org/10.3390/molecules22010130>
- [21] Kaya, İ., Er, G. and Temizkan, K. (2018) Synthesis, Characterization and Fluorescence Properties of Azomethine Polymer Containing Quinoline Unit. *Polymer Bulletin*, **75**, 1809-1822. <https://doi.org/10.1007/s00289-017-2125-9>
- [22] Li, W.-H., He, Q., Zhang, S.-T., Pei, C.-L. and Hou, B.-R. (2008) Some New Triazole Derivatives as Inhibitors for Mild Steel Corrosion in Acidic Medium. *Journal of Applied Electrochemistry*, **38**, 289-295. <https://doi.org/10.1007/s10800-007-9437-7>
- [23] Saady, A., Rais, Z., Benhiba, F., Salim, R., Ismaily Alaoui, K., Arrousse, N., *et al.*

- (2021) Chemical, Electrochemical, Quantum, and Surface Analysis Evaluation on the Inhibition Performance of Novel Imidazo [4,5-b] Pyridine Derivatives against Mild Steel Corrosion. *Corrosion Science*, **189**, Article ID: 109621. <https://doi.org/10.1016/j.corsci.2021.109621>
- [24] Zhao, M.-C., Liu, M., Song, G.-L. and Atrens, A. (2008) Influence of pH and Chloride Ion Concentration on the Corrosion of Mg Alloy ZE41, *Corrosion Science*, **50**, 3168-3178. <https://doi.org/10.1016/j.corsci.2008.08.023>
- [25] Zheng, X., Zhang, S., Li, W., Yin, L., He, J. and Wu, J. (2014) Investigation of 1-butyl-3-methyl-1H-benzimidazolium Iodide as Inhibitor for Mild Steel in Sulfuric Acid Solution. *Corrosion Science*, **80**, 383-392. <https://doi.org/10.1016/j.corsci.2013.11.053>
- [26] Dutta, A., Saha, S.K., Adhikari, U., Banerjee, P. and Sukul, D. (2017) Effect of Substitution on Corrosion Inhibition Properties of 2-(Substituted Phenyl) Benzimidazole Derivatives on Mild Steel in 1 M HCl Solution: A Combined Experimental and Theoretical Approach. *Corrosion Science*, **123**, 256-266. <https://doi.org/10.1016/j.corsci.2017.04.017>
- [27] Lebrini, M., Robert, F. and Roos, C. (2010) Inhibition Effect of Alkaloids Extract from *Annona squamosa* Plant on the Corrosion of C38 Steel in Normal Hydrochloric Acid Medium. *International Journal of Electrochemical Science*, **5**, 1698-1712.
- [28] Gao, L., Peng, S., Huang, X. and Gong, Z. (2020) A Combined Experimental and Theoretical Study of Papain as a Biological Eco-Friendly Inhibitor for Copper Corrosion in H₂SO₄ Medium. *Applied Surface Science*, **511**, Article ID: 145446. <https://doi.org/10.1016/j.apsusc.2020.145446>
- [29] Hu, Z., Meng, Y., Ma, X., Zhu, H., Li, J., Li, C., *et al.* (2016) Experimental and Theoretical Studies of Benzothiazole Derivatives as Corrosion Inhibitors for Carbon Steel in 1 M HCl. *Corrosion Science*, **112**, 563-575. <https://doi.org/10.1016/j.corsci.2016.08.012>
- [30] Tan, B., Zhang, S., Liu, H., Qiang, Y., Li, W., Guo, L., *et al.* (2019) Insights into the Inhibition Mechanism of Three 5-Phenyltetrazole Derivatives for Copper Corrosion in Sulfuric Acid Medium via Experimental and DFT Methods. *Journal of the Taiwan Institute of Chemical Engineers*, **102**, 424-437. <https://doi.org/10.1016/j.jtice.2019.06.005>
- [31] Li, Y., Zhang, S., Ding, Q., Qin, B. and Hu, L. (2019) Versatile 4,6-dimethyl-2-mercaptopyrimidine Based Ionic Liquids as High-Performance Corrosion Inhibitors and Lubricants. *Journal of Molecular Liquids*, **284**, 577-585. <https://doi.org/10.1016/j.molliq.2019.04.042>
- [32] Li, X., Deng, S., Lin, T., Xie, X. and Du, G. (2017) 2-Mercaptopyrimidine as an Effective Inhibitor for the Corrosion of Cold Rolled Steel in HNO₃ Solution. *Corrosion Science*, **118**, 202-216. <https://doi.org/10.1016/j.corsci.2017.02.011>
- [33] Talari, M., Nezhad, S.M., Alavi, S.J., Mohtashampour, M., Davoodi, A. and Hosseinpour, S. (2019) Experimental and Computational Chemistry Studies of Two Imidazole-Based Compounds as Corrosion Inhibitors for Mild Steel in HCl Solution. *Journal of Molecular Liquids*, **286**, Article ID: 110915. <https://doi.org/10.1016/j.molliq.2019.110915>
- [34] Zhang, Z., Tian, N., Zhang, W., *et al.* (2016) Inhibition of Carbon Steel Corrosion in Phase-Change-Materials Solution by Methionine and Proline. *Corrosion Science*, **111**, 675-689. <https://doi.org/10.1016/j.corsci.2016.06.005>
- [35] Musa, A.Y., Kadhum, A.A.H., Mohamad, A.B., *et al.* (2010) Experimental and Theoretical Study on the Inhibition Performance of Triazole Compounds for Mild

- Steel Corrosion. *Corrosion Science*, **52**, 3331-3340.
<https://doi.org/10.1016/j.corsci.2010.06.002>
- [36] Lgaz, H., Chaouiki, A., Chafiq, M., *et al.* (2021) Evaluating the Corrosion Inhibition Properties of Novel 1,2,3-triazolyl Nucleosides and Their Synergistic Effect with Iodide Ions against Mild Steel Corrosion in HCl: A Combined Experimental and Computational Exploration. *Journal of Molecular Liquids*, **338**, Article ID: 116522.
<https://doi.org/10.1016/j.molliq.2021.116522>
- [37] Lee, D.Y., Kim, W.C. and Kim, J.G. (2012) Effect of Nitrite Concentration on the Corrosion Behaviour of Carbon Steel Pipelines in Synthetic Tap Water. *Corrosion Science*, **64**, 105-114. <https://doi.org/10.1016/j.corsci.2012.07.005>
- [38] Kallip, S., Bastos, A.C., Yasakau, K.A., *et al.* (2012) Synergistic Corrosion Inhibition on Galvanically Coupled Metallic Materials. *Electrochemistry Communications*, **20**, 101-104. <https://doi.org/10.1016/j.elecom.2012.04.007>
- [39] Javadian, S., Yousefi, A. and Neshati, J. (2013) Synergistic Effect of Mixed Cationic and Anionic Surfactants on the Corrosion Inhibitor Behavior of Mild Steel in 3.5% NaCl. *Applied Surface Science*, **285**, 674-681.
<https://doi.org/10.1016/j.apsusc.2013.08.109>
- [40] Zhang, Z., Tian, N., Li, X., *et al.* (2015) Synergistic Inhibition Behavior between Indigo Carmine and Cetyl Trimethyl Ammonium Bromide on Carbon Steel Corroded in a 0.5 M HCl Solution. *Applied Surface Science*, **357**, 845-855.
<https://doi.org/10.1016/j.apsusc.2015.09.092>
- [41] Issaadi, S., Douadi, T., Zouaoui, A., *et al.* (2011) Novel Thiophene Symmetrical Schiff Base Compounds as Corrosion Inhibitor for Mild Steel in Acidic Media. *Corrosion Science*, **53**, 1484-1488. <https://doi.org/10.1016/j.corsci.2011.01.022>
- [42] Obot, I.B., Ebenso, E.E. and Kabanda, M.M. (2013) Metronidazole as Environmentally Safe Corrosion Inhibitor for Mild Steel in 0.5 M HCl: Experimental and Theoretical Investigation. *Journal of Environmental Chemical Engineering*, **1**, 431-439.
<https://doi.org/10.1016/j.jece.2013.06.007>
- [43] Yıldız, R., Döner, A., Doğan, T. and Dehri, İ. (2014) Experimental Studies of 2-Pyridinecarbonitrile as Corrosion Inhibitor for Mild Steel in Hydrochloric Acid Solution. *Corrosion Science*, **82**, 125-132.
<https://doi.org/10.1016/j.corsci.2014.01.008>
- [44] Tao, Z., Zhang, S., Li, W., *et al.* (2009) Corrosion Inhibition of Mild Steel in Acidic Solution by Some Oxo-Triazole Derivatives. *Corrosion Science*, **51**, 2588-2595.
<https://doi.org/10.1016/j.corsci.2009.06.042>
- [45] Salman, M., Ansari, K.R., Haque, J., Srivastava, V., Quraishi, M.A., Mazumder, M.A.J., *et al.* (2020) Ultrasound-Assisted Synthesis of Substituted Triazines and Their Corrosion Inhibition Behavior on N80 Steel/Acid Interface. *Journal of Heterocyclic Chemistry*, **57**, 2157-2172. <https://doi.org/10.1002/jhet.3936>
- [46] Yang, K., Peng, H., Wen, Y. and Li, N. (2010) Re-Examination of Characteristic FTIR Spectrum of Secondary Layer in Bilayer Oleic Acid-Coated Fe₃O₄ Nanoparticles. *Applied Surface Science*, **256**, 3093-3097.
<https://doi.org/10.1016/j.apsusc.2009.11.079>
- [47] Ruan, H., Frost, R., Klopogge, J. and Duong, L. (2002) Infrared Spectroscopy of Goethite Dehydroxylation: III. FT-IR Microscopy of *in Situ* Study of the Thermal Transformation of Goethite to Hematite. *Spectrochimica Acta Part A: Molecular and Biomolecular Spectroscopy*, **58**, 967-981.
[https://doi.org/10.1016/S1386-1425\(01\)00574-1](https://doi.org/10.1016/S1386-1425(01)00574-1)
- [48] Cornell, R.M. and Schwertmann, U. (2003) The Iron Oxides: Structure, Properties,

Reactions, Occurrences and Uses. 2nd Edition, John Wiley & Sons, Germany.

<https://doi.org/10.1002/3527602097>

- [49] Muthukrishnan, P., Prakash, P., Jeyaprabha, B., *et al.* (2019) Stigmasterol Extracted from *Ficus hispida* Leaves as a Green Inhibitor for the Mild Steel Corrosion in 1 M HCl Solution. *Arabian Journal of Chemistry*, **12**, 3345-3356. <https://doi.org/10.1016/j.arabjc.2015.09.005>
- [50] Chung, I.-M., Kalaiselvi, K., Sasireka, A., *et al.* (2018) Anticorrosive Property of *Spiraea Cantonensis* Extract as an Eco-Friendly Inhibitor on Mild Steel Surface in Acid Medium. *Journal of Dispersion Science and Technology*, **40**, 1326-1337. <https://doi.org/10.1080/01932691.2018.1511435>
- [51] Muthukrishnan, P., Jeyaprabha, B., Tharmaraj, P., *et al.* (2015) Inhibition of the Corrosion of Mild Steel in Acidic Media by Use of a New Antipyridine Derivative. *Research on Chemical Intermediates*, **41**, 5961-5984. <https://doi.org/10.1007/s11164-014-1714-6>
- [52] Bereket, G., Hür, E. and Öğretir, C. (2002) Quantum Chemical Studies on Some Imidazole Derivatives as Corrosion Inhibitors for Iron in Acidic Medium. *Journal of Molecular Structure: THEOCHEM*, **578**, 79-88. [https://doi.org/10.1016/S0166-1280\(01\)00684-4](https://doi.org/10.1016/S0166-1280(01)00684-4)
- [53] Zhang, K., Xu, B., Yang, W., *et al.* (2015) Halogen-Substituted Imidazoline Derivatives as Corrosion Inhibitors for Mild Steel in Hydrochloric Acid Solution. *Corrosion Science*, **90**, 284-295. <https://doi.org/10.1016/j.corsci.2014.10.032>
- [54] Dutta, A., Saha, S.K., Banerjee, P., *et al.* (2015) Correlating Electronic Structure with Corrosion Inhibition Potentiality of Some Bis-Benzimidazole Derivatives for Mild Steel in Hydrochloric Acid: Combined Experimental and Theoretical Studies. *Corrosion Science*, **98**, 541-550. <https://doi.org/10.1016/j.corsci.2015.05.065>
- [55] Kokalj, A. (2010) Is the Analysis of Molecular Electronic Structure of Corrosion Inhibitors Sufficient to Predict the Trend of Their Inhibition Performance. *Electrochimica Acta*, **56**, 745-755. <https://doi.org/10.1016/j.electacta.2010.09.065>